

Measurements of neutron energy spectra of ${}^9\text{Be}(d,n){}^{10}\text{B}$ reaction with a thick beryllium target*

Shuang-Jiao Zhang(张双佼)¹ Zhi-Jie Hu(胡志杰)¹ Zhi-Ming Hu(户志鸣)¹ Chao Han(韩超)¹
 Xiao-Hou Bai(白晓厚)¹ Chang-Qi Liu(刘昌奇)¹ Chang Huang(黄畅)¹ Qin Xie(谢芹)¹ Dong-Ying Huo(霍东英)¹
 Kang Wu(吴康)¹ Yang-Bo Nie(聂阳波)³ Yan-Yan Ding(丁琰琰)³ Kai Zhang(张凯)³ Yu Zhang(张宇)^{1,2}
 Zhi-Yong Deng(邓志勇)⁴ Rui Guo(郭锐)⁴ Zheng Wei(韦峥)^{1,2†} Ze-En Yao(姚泽恩)^{1,2‡}

¹School of Nuclear Science and Technology, Lanzhou University, Lanzhou 730000, China

²Engineering Research Center for Neutron Application Technology, Ministry of Education, Lanzhou University, Lanzhou 730000, China

³Key Laboratory of Nuclear Data, China Institute of Atomic Energy, Beijing 102413, China

⁴Nuclear Power Institute of China, Chengdu 610000, China

Abstract: Novel measurements of the neutron energy spectra of the ${}^9\text{Be}(d,n){}^{10}\text{B}$ reaction with a thick beryllium target are performed using a fast neutron time-of-flight (TOF) spectrometer for the neutron emission angles $\theta = 0^\circ$ and 45° , and the incident deuteron energies are 250 and 300 keV, respectively. The neutron contributions from the ${}^9\text{Be}(d,n){}^{10}\text{B}$ reaction are distributed relatively independently for the ground state and the first, second, and third excited states of ${}^{10}\text{B}$. The branching ratios of the ${}^9\text{Be}(d,n){}^{10}\text{B}$ reaction for the different excited states of ${}^{10}\text{B}$ are obtained for the neutron emission angles $\theta = 0^\circ$ and 45° , and the incident deuteron energies are 250 and 300 keV, respectively. The branching ratio of the ${}^9\text{Be}(d,n){}^{10}\text{B}$ reaction for the third excited state decreases with increase in the incident deuteron energy, and the branching ratios for the ground state and the second excited state increase with increase in the neutron emission angle.

Keywords: neutron energy spectrum, branching ratio, ${}^9\text{Be}(d,n){}^{10}\text{B}$ reaction, neutron time-of-flight spectrometer

DOI: 10.1088/1674-1137/abce13

I. INTRODUCTION

Accelerator neutron sources are widely used in neutron physics and neutron applications, owing to the high neutron yield, good controllability, compactness, and nonproliferation capability [1-9]. Typically, in exothermic nuclear reactions, deuterons and tritons are bombarded with deuterium ions, producing fusion neutrons by the ${}^2\text{H}(d,n){}^3\text{He}$ (D-D) and ${}^3\text{H}(d,n){}^4\text{He}$ (D-T) reactions, and deuterium ions bombard beryllium, producing neutrons by the ${}^9\text{Be}(d,n){}^{10}\text{B}$ (D-Be) reaction for low energy D^+ ions at $\sim 10^2$ keV.

Compared with deuterium-adsorption targets and tritium-adsorption targets, metallic beryllium exhibits stable chemical properties and excellent hardness. Pure metallic beryllium targets are easy to obtain, and they can be easily processed into various shapes. Beryllium has a high melting point (1280 °C) and good thermal conduction,

which allows metallic beryllium targets to withstand high intensity D^+ ion beams. Most importantly, the cross section of the ${}^2\text{H}(d,n){}^3\text{He}$ (D-D) reaction is roughly equivalent to the ${}^9\text{Be}(d,n){}^{10}\text{B}$ (D-Be) reaction for low energy D^+ ions at $\sim 10^2$ keV. As a result, accelerator-based ${}^9\text{Be}(d,n){}^{10}\text{B}$ reaction neutron sources can generate high intensity and continuous-spectrum neutron fields at low energy deuterium ions.

The ${}^9\text{Be}(d,n){}^{10}\text{B}$ reaction is relatively complex. For low-energy deuterium ions, ${}^9\text{Be}(d,n){}^{10}\text{B}$ is an exothermic reaction with $Q = +4.36$ MeV, but there are four well-known excitation states of ${}^{10}\text{B}$ [10, 11]. With increasing energy of deuterium ions, several many-body reactions (${}^9\text{Be}(d,2n){}^9\text{B}$ ($Q = -4.1$ MeV), ${}^9\text{Be}(d,np){}^9\text{Be}$ ($Q = -2.2$ MeV), and ${}^9\text{Be}(d,2np){}^8\text{Be}$ ($Q = -3.8$ MeV)) markedly enhance the neutron yield and extend the neutron energy spectrum. However, measurements of the neutron energy

Received 7 August 2020; Accepted 28 October 2020; Published online 14 December 2020

* Supported by the National Natural Science Foundation of China (11875155, 11705071, 12075105), the NSFC-Nuclear Technology Innovation Joint Fund (U1867213), the NSAF (U1830102), the Fundamental Research Funds for the Central Universities of China (lzujbky-2020-kb09) and the Project of National Defense Science and Technology Industry for Nuclear Power Technology Innovation Center (HDLXZX-2019-HD-33)

[†] E-mail: weizheng@lzu.edu.cn

[‡] E-mail: zeyao@lzu.edu.cn

©2021 Chinese Physical Society and the Institute of High Energy Physics of the Chinese Academy of Sciences and the Institute of Modern Physics of the Chinese Academy of Sciences and IOP Publishing Ltd

spectra, angular distribution, and integrated yields for the ${}^9\text{Be}(d,xn)$ reaction have been scarce, and the existing studies mainly focus on the deuterium ion energies from a few MeV to tens of MeV [10-36]. Some notable exceptions are a study by Coombe *et al.*, who measured the neutron energy spectra from the ${}^9\text{Be}(d,n){}^{10}\text{B}$ reaction for 80 keV deuterium ions at 0° and 45° [37], and a study by Zou *et al.*, who measured the angular distribution and neutron yields from the ${}^9\text{Be}(d,n){}^{10}\text{B}$ reaction for 200 and 500 keV deuterium ions [38].

The ${}^9\text{Be}(d,n){}^{10}\text{B}$ reaction is a typical direct reaction, and the angular distribution of the ${}^9\text{Be}(d,n){}^{10}\text{B}$ neutron source presents a forward trend. Neutrons from direct reaction mechanisms are still visible at larger neutron emission angles, but the relative intensity and the positions of maxima decrease with the angle. Consequently, it is more beneficial to select forward angles for studying the branching ratio of the ${}^9\text{Be}(d,n){}^{10}\text{B}$ reaction.

In this work, novel measurements of the neutron energy spectra of the ${}^9\text{Be}(d,n){}^{10}\text{B}$ reaction with a thick beryllium target were performed for the neutron emission angles of $\theta = 0^\circ$ and 45° , and the respective incident deuterium energies were 250 and 300 keV. This work provides basic information for accelerator-based D-Be neutron sources used in neutron physics and neutron applications.

II. EXPERIMENT

A. Experimental arrangement

The measurements of the neutron energy spectra of the ${}^9\text{Be}(d,n){}^{10}\text{B}$ reaction with a thick beryllium target for low energy deuterium ions were performed using a fast neutron time-of-flight (TOF) spectrometer and a Cockcroft-Walton accelerator at the China Institute of Atomic Energy (CIAE). The experimental setup is shown in Fig. 1. The Cockcroft-Walton accelerator provided D^+ ions at 250 and 300 keV with a frequency of 1.5 MHz and pulse width of 2.5 ns. The target used in this experiment was a pure metallic beryllium sample with a diameter of 22.0 mm and thickness of 1.0 mm in the 0° direction with respect to the deuterium beam.

The fast neutron TOF spectrometer was employed at 0° and 45° for measuring the neutron energy spectra of the ${}^9\text{Be}(d,n){}^{10}\text{B}$ reaction. The spectrometer consisted of a BC501A liquid scintillator with a diameter of 5.08 cm and thickness of 2.54 cm, and a HAMAMATSU R329-02 photomultiplier tube. The flight length of the emitted neutrons between the metallic beryllium target and the front surface of the detector was 3.0 m. In this experiment, the threshold of the BC501A liquid scintillator detector was 0.191 MeV. A silicon surface barrier detector (SSD) was placed in the 135° direction with respect to the

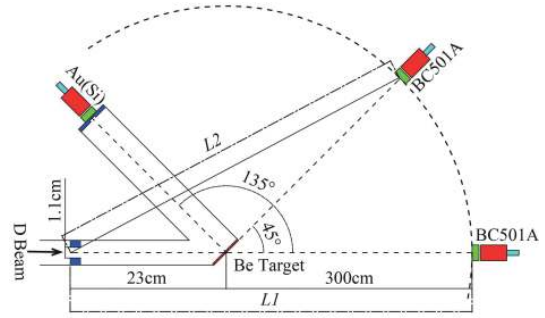


Fig. 1. (color online) The experimental setup for measuring the neutron energy spectra of the ${}^9\text{Be}(d,n){}^{10}\text{B}$ reaction.

deuteron beam, to monitor the neutron yield by counting the associated protons from the $D(d,p)\text{T}$ reaction owing to the deuterium ions bombarding self-injecting deuterons in the target, because the $D(d,n){}^3\text{He}$ reaction occurred along with the $D(d,p)\text{T}$ reaction. The SSD was positioned at 90 cm from the Be sample target.

In addition, the deuteron beam self-injected into a beam-limiting diaphragm, and deuterium ions bombarded self-injected deuterons in the beam-limiting diaphragm, to produce neutrons by the $D(d,n){}^3\text{He}$ reaction. These neutrons were also responded to in the BC501A liquid scintillator detector. To determine the position of the $D(d,n){}^3\text{He}$ neutron peaks in the neutron TOF spectra and neutron energy spectra, the neutron flight distances from the beam-limiting diaphragm to the BC501A liquid scintillator detector are shown in Fig. 1. $L1$ is the neutron flight distance at 0° , which was 3.230 m. $L2$ is the flight distance at 45° , which was 3.134 m.

In the experiment, all of the events that were detected by the detector were recorded in a list mode on a single event basis, using a CAMAC data acquisition system. Each event was characterized by three parameters: the pulse height (PH), pulse shape discrimination (PSD), and TOF. The PH and PSD parameters were used for the detection threshold determination and n- γ discrimination, respectively, in the offline analysis.

B. TOF spectra

As shown in Fig. 1, the BC501A liquid scintillator detector was used as the primary detector in the experiment, for measuring the neutron spectra. Although the BC501A liquid scintillator detector is sensitive to both neutrons and gamma rays, the output pulse shapes for neutrons and gamma rays in liquid scintillator detectors are different, allowing to distinguish neutron and gamma signals. In this work, a 4-channel pulse shape discriminator was used for distinguishing the detected neutron and gamma signals using the zero-crossing time method for all measured TOF, and gamma signals were rejected. Neutron-only TOF spectra were obtained by filtering the mixture TOF spectra of neutrons and gamma rays, choosing neutron signals in the two-dimensional distributions

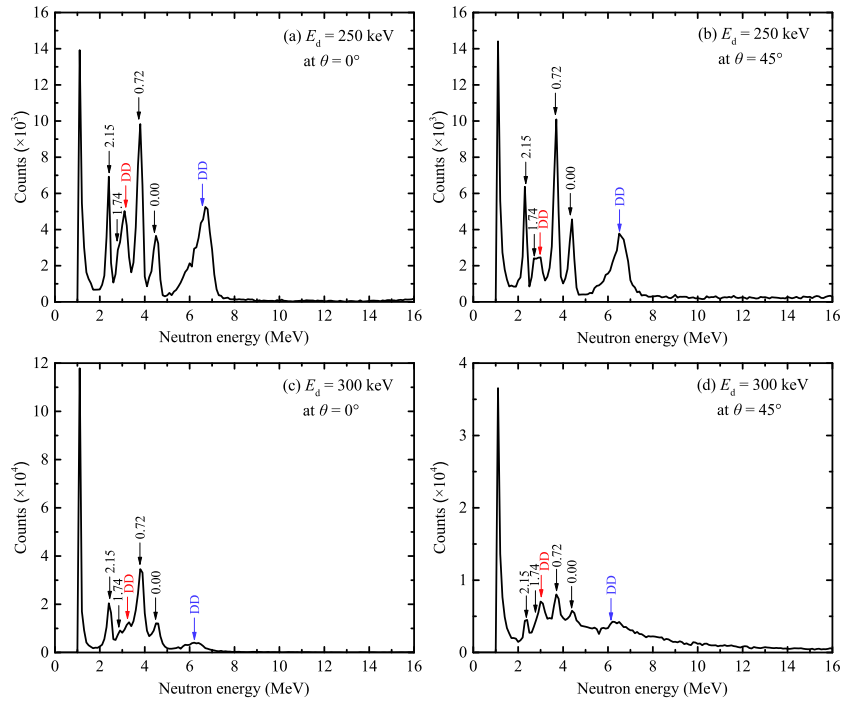


Fig. 3. (color online) The measured neutron energy spectra of the ${}^9\text{Be}(d,n){}^{10}\text{B}$ reaction, for deuteron energies of 250 and 300 keV and neutron emission angles of 0° and 45° , respectively. Arrows indicate the results of the calculations. The red arrow marks the energy of the neutrons from the $\text{D}(d,n){}^3\text{He}$ reaction, for the metallic beryllium target. The violet arrow marks the energy of the neutrons from the $\text{D}(d,n){}^3\text{He}$ reaction, for the beam-limiting diaphragm. The black arrows mark the energies of the neutrons from the ${}^9\text{Be}(d,n){}^{10}\text{B}$ reaction, for ${}^{10}\text{B}$ in different excited states.

the neutron detection efficiency of the BC501A liquid scintillator detector, calculated using the NEFF code [39].

As for the ${}^9\text{Be}(d,n){}^{10}\text{B}$ reaction, emitted neutrons had different energies, because ${}^{10}\text{B}$ can be in different excited states [15, 20]. The excited states of ${}^{10}\text{B}$ are 0, 0.72, 1.74, 2.15, 3.58, and 5.17 MeV, corresponding to the Q -energies of 4.36, 3.64, 2.62, 2.21, 0.78, and -0.81 MeV, respectively. The energies of the emitted neutrons for the different excited states of ${}^{10}\text{B}$ can be calculated using the Q -equation [40]

$$E_n = \frac{m_d \times m_n}{(m_n + m_B)^2} \times E_d \times \left[\cos\theta_L \pm \sqrt{\cos^2\theta_L + \frac{m_n + m_B}{m_d \cdot m_n} \left(m_B - m_d + \frac{Q}{E_d} \cdot m_B \right)} \right]^2, \quad (2)$$

where E_d is the incident deuteron energy, and m_d , m_n , and m_B denote the masses of the deuteron, neutron, and boron, respectively. Q is the Q -energy of the ${}^9\text{Be}(d,n){}^{10}\text{B}$ reaction, and θ_L is the neutron emission angle in the laboratory system.

The measured neutron energy spectra of the ${}^9\text{Be}(d,n){}^{10}\text{B}$ reaction, for deuteron energies of 250 keV and 300 keV and neutron emission angles of 0° and 45° , are shown in Fig. 3. We observe six typical neutron en-

ergy peaks, corresponding to the neutrons from the $\text{D}(d,n){}^3\text{He}$ reaction for the beam-limiting diaphragm, neutrons from the ${}^9\text{Be}(d,n){}^{10}\text{B}$ reaction for the ground state of ${}^{10}\text{B}$ ($Q = 4.36$ MeV), neutrons from the ${}^9\text{Be}(d,n){}^{10}\text{B}$ reaction for the first excited state of ${}^{10}\text{B}$ ($Q = 3.64$ MeV), neutrons from the $\text{D}(d,n){}^3\text{He}$ reaction for the metallic beryllium target, neutrons from the ${}^9\text{Be}(d,n){}^{10}\text{B}$ reaction for the second excited state of ${}^{10}\text{B}$ ($Q = 2.62$ MeV), and neutrons from the ${}^9\text{Be}(d,n){}^{10}\text{B}$ reaction for the third excited state of ${}^{10}\text{B}$ ($Q = 2.21$ MeV) [peak positions from right to left]. The neutron energy peak corresponding to the neutrons from the ${}^9\text{Be}(d,n){}^{10}\text{B}$ reaction for the fourth excited state of ${}^{10}\text{B}$ ($Q = 0.78$ MeV) has very high counts owing to the modification of the small neutron detection efficiency at 1.1 MeV. Owing to the large uncertainty of detection efficiency for neutrons at 1.1 MeV, this neutron energy peak was not analyzed. To validate the accuracy of the measured neutron energy spectra of the ${}^9\text{Be}(d,n){}^{10}\text{B}$ reaction, the neutron energies for the ${}^9\text{Be}(d,n){}^{10}\text{B}$ reaction and the $\text{D}(d,n){}^3\text{He}$ reaction were calculated using the Q -equation, and the results are marked by arrows in Fig. 3. The calculated neutron energies and the neutron peak position energies in the measured neutron energy spectra of the ${}^9\text{Be}(d,n){}^{10}\text{B}$ reaction are compared in Table 1. The relative deviation (RD) between the calculated neutron energy and the neutron peak position energy can be used for validating the accuracy of the

measured neutron energy spectra of the ${}^9\text{Be}(d,n){}^{10}\text{B}$ reaction and can be calculated using the following equation:

$$\text{RD} = 100 \times \left| \frac{E_{\text{exp}} - E_{\text{cal}}}{E_{\text{cal}}} \right|, \quad (3)$$

where E_{cal} is the calculated neutron energy, and E_{exp} is the neutron peak position energy in the measured neutron energy spectra. Table 1 shows that the maximal relative deviation is 2.17%, validating the accuracy of the experimentally measured neutron energy spectra of the ${}^9\text{Be}(d,n){}^{10}\text{B}$ reaction.

As shown in Fig. 3, neutrons from the $\text{D}(d,n){}^3\text{He}$ reaction for the metallic beryllium target significantly affect the neutron energy spectra distributions of the ${}^9\text{Be}(d,n){}^{10}\text{B}$ reaction. It is necessary to exclude the neutrons from the $\text{D}(d,n){}^3\text{He}$ reaction for the metallic beryllium target from the neutron energy spectra of the ${}^9\text{Be}(d,n){}^{10}\text{B}$ reaction. To achieve this, we replaced the

Table 1. Comparison of the calculated neutron energies and the experimental results for the ${}^9\text{Be}(d,n){}^{10}\text{B}$ reaction.

E_d/angle	states	$E_{\text{cal}}/\text{MeV}$	$E_{\text{exp}}/\text{MeV}$	RD (%)
250 keV/ 0°	DD	6.58	6.7	1.82
	0.00	4.42	4.5	1.81
	0.72	3.74	3.8	1.60
	DD	3.15	3.1	1.59
	1.74	2.78	–	–
	2.15	2.39	2.4	0.42
250 keV/ 45°	DD	6.52	6.5	0.31
	0.00	4.33	4.4	1.62
	0.72	3.66	3.7	1.09
	DD	2.95	3.0	1.69
	1.74	2.71	2.7	0.37
	2.15	2.33	2.3	1.29
300 keV/ 0°	DD	6.21	6.2	0.16
	0.00	4.48	4.5	0.45
	0.72	3.80	3.8	0.00
	DD	3.23	3.3	2.17
	1.74	2.84	2.9	2.11
	2.15	2.45	2.4	2.04
300 keV/ 45°	DD	6.12	6.2	1.31
	0.00	4.39	4.4	0.23
	0.72	3.72	3.7	0.54
	DD	3.01	3.0	0.33
	1.74	2.77	–	–
	2.15	2.38	2.4	0.84

metallic beryllium target with a thick deuterium-adsorption target. The Cockcroft-Walton accelerator generated D^+ ions, which bombarded the thick deuterium-adsorption target to produce only D-D neutrons. The fast neutron TOF spectrometer was employed for measuring the energy spectra of the neutrons from the $\text{D}(d,n){}^3\text{He}$ reaction, and the SSD was used for counting the associated protons generated in the $\text{D}(d,p)\text{T}$ reaction that occurred along with the $\text{D}(d,n){}^3\text{He}$ reaction, as shown in Fig. 1.

Figure 4 shows the measured neutron energy spectrum for the $\text{D}(d,n){}^3\text{He}$ reaction, for the deuteron energy of 300 keV and neutron emission angle of 0° , as an example. Clearly, there are two neutron peaks in this spectrum. The right peak is the main peak of D-D neutrons, for the neutron energy of 3.23 MeV, which agrees well with the result calculated using the Q -equation. The left peak is contributed by the D-D neutrons that are slowed down and scattered.

Because the $\text{D}(d,n){}^3\text{He}$ reaction is accompanied by the $\text{D}(d,p)\text{T}$ reaction, the SSD can measure the associated protons, for monitoring the neutron yields of the $\text{D}(d,n){}^3\text{He}$ reaction. With either the metallic beryllium target (self-injecting deuterons into the target) or the deuterium-adsorption target, associated protons from the $\text{D}(d,p)\text{T}$ reaction can serve as a normalized standard. In excluding the neutrons from the $\text{D}(d,n){}^3\text{He}$ reaction for the metallic beryllium target from the neutron energy spectrum of the ${}^9\text{Be}(d,n){}^{10}\text{B}$ reaction, the experimentally measured $\text{D}(d,n){}^3\text{He}$ neutron spectrum and ${}^9\text{Be}(d,n){}^{10}\text{B}$ neutron spectrum should be normalized by proton counts measured by the SSD at 135° . The normalized ${}^9\text{Be}(d,n){}^{10}\text{B}$ neutron energy spectrum, excluding the effect of the neutrons from the $\text{D}(d,n){}^3\text{He}$ reaction, can be obtained by subtracting the normalized $\text{D}(d,n){}^3\text{He}$ neutron energy spectrum from the normalized ${}^9\text{Be}(d,n){}^{10}\text{B}$ neutron energy spectrum and can be calculated using the

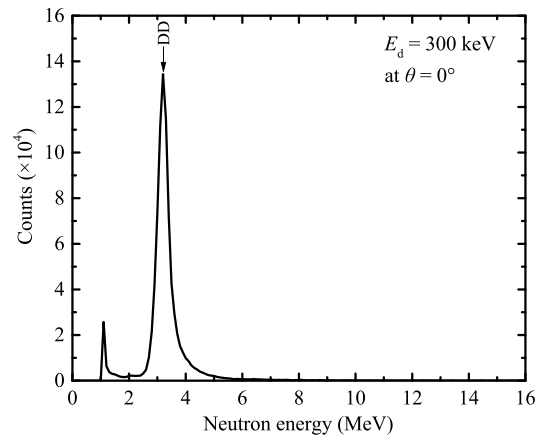


Fig. 4. The measured neutron energy spectrum of the $\text{D}(d,n){}^3\text{He}$ reaction, for a deuteron energy of 300 keV and neutron emission angle of 0° . The black arrow denotes the calculated neutron energy for the $\text{D}(d,n){}^3\text{He}$ reaction.

following equation:

$$n_{\text{net}} = \frac{N_{\text{Be_target}}}{N(SSD)_{\text{Be_target}}} - \frac{N_{\text{D_target}}}{N(SSD)_{\text{D_target}}}, \quad (4)$$

where n_{net} is the normalized ${}^9\text{Be}(d,n){}^{10}\text{B}$ neutron energy spectrum, excluding the effect of the $\text{D}(d,n){}^3\text{He}$ reaction neutrons. $N_{\text{Be_target}}$ and $N(SSD)_{\text{Be_target}}$ represent the measured neutron energy spectrum of the ${}^9\text{Be}(d,n){}^{10}\text{B}$ reaction and the counts of associated protons for the beryllium target. $N_{\text{D_target}}$ and $N(SSD)_{\text{D_target}}$ represent the measured neutron energy spectrum of the $\text{D}(d,n){}^3\text{He}$ reaction and the counts of associated protons for the deuterium-absorption target. Typical results are shown in Fig. 5. Clearly, the $\text{D}(d,n){}^3\text{He}$ reaction neutron peak at 3.23 MeV is excluded from the ${}^9\text{Be}(d,n){}^{10}\text{B}$ neutron spectrum, validating the method for excluding the $\text{D}(d,n){}^3\text{He}$ reaction neutrons. It should be emphasized that, as shown in Fig. 5, the rightmost peak corresponds to the neutrons from the $\text{D}(d,n){}^3\text{He}$ reaction for the beam-limiting diaphragm, which do not affect the neutron energy spectrum distribution for the ${}^9\text{Be}(d,n){}^{10}\text{B}$ reaction on the different excited states of ${}^{10}\text{B}$.

Based on the above-mentioned data analysis method, the measured neutron energy spectra of the ${}^9\text{Be}(d,n){}^{10}\text{B}$ reaction, excluding neutrons of the $\text{D}(d,n){}^3\text{He}$ reaction for the metallic beryllium target, for deuteron energies of 250 and 300 keV and neutron emission angles of 0° and 45° , are shown in Fig. 6. The neutron contributions from the ${}^9\text{Be}(d,n){}^{10}\text{B}$ reaction are distributed relatively independently for different excited states of ${}^{10}\text{B}$ (from right to left:

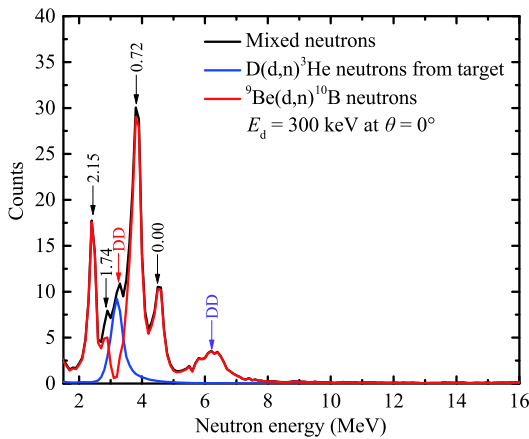


Fig. 5. (color online) The normalized ${}^9\text{Be}(d,n){}^{10}\text{B}$ neutron energy spectrum, excluding the neutrons of the $\text{D}(d,n){}^3\text{He}$ reaction for the metallic beryllium target, for a deuteron energy of 300 keV and neutron emission angle of 0° . The arrows indicate the calculated neutron energies. The red and violet arrows denote the neutrons from the $\text{D}(d,n){}^3\text{He}$ reaction for the metallic beryllium target and the beam-limiting diaphragm, respectively, and the black arrows are the neutrons from the ${}^9\text{Be}(d,n){}^{10}\text{B}$ reaction, for ${}^{10}\text{B}$ in different excited states.

the ground state ($Q = 4.36$ MeV), first excited state ($Q = 3.64$ MeV), second excited state ($Q = 2.62$ MeV), and third excited state ($Q = 2.21$ MeV) of ${}^{10}\text{B}$.

Neutrons from the $\text{D}(d,n){}^3\text{He}$ reaction for the beam-limiting diaphragm cannot be excluded, causing higher background in measured neutron energy spectra of the ${}^9\text{Be}(d,n){}^{10}\text{B}$ reaction. According to the beam dynamics of the accelerator, with increasing energy of incident deuterons, the number of neutrons from the $\text{D}(d,n){}^3\text{He}$ reaction for the beam-limiting diaphragm continues to increase owing to the space charge effects of deuterium ions, particularly at large neutron emission angles. Obviously, the background in Fig. 6(d) is higher than those in Fig. 6(a)-6(c).

From data analysis, the branching ratios of the ${}^9\text{Be}(d,n){}^{10}\text{B}$ reaction were obtained for the different excited states of ${}^{10}\text{B}$, and the results are shown in Fig. 6. The branching ratios of the ${}^9\text{Be}(d,n){}^{10}\text{B}$ reaction for the ground state, first excited state, second excited state, and third excited state are 48.21%, 100.00%, 11.99%, and 39.11%, respectively, for a deuteron energy of 250 keV and neutron emission angle of 0° . The branching ratios of the ${}^9\text{Be}(d,n){}^{10}\text{B}$ reaction for the ground state, first excited state, second excited state, and third excited state are 58.61%, 100.00%, 12.43%, and 37.71%, respectively, for a deuteron energy of 250 keV and neutron emission angle of 45° . The branching ratios of the ${}^9\text{Be}(d,n){}^{10}\text{B}$ reaction for the ground state, first excited state, second excited state, and third excited state are 45.61%, 100.00%, 11.65%, and 32.61%, respectively, for a deuteron energy of 300 keV and neutron emission angle of 0° . The branching ratios of the ${}^9\text{Be}(d,n){}^{10}\text{B}$ reaction for the ground state, first excited state, second excited state, and third excited state are 91.85%, 100.00%, 18.31%, and 32.98%, respectively, for a deuteron energy of 300 keV and neutron emission angle of 45° . With increasing incident deuteron energy, the branching ratio of the ${}^9\text{Be}(d,n){}^{10}\text{B}$ reaction for the third excited state clearly decreases. With increasing neutron emission angle, the branching ratios for the ground state and the second excited state increase.

The statistical error (SE) of the measured neutron energy spectra of the ${}^9\text{Be}(d,n){}^{10}\text{B}$ reaction, excluding the neutrons from the $\text{D}(d,n){}^3\text{He}$ reaction for the metallic beryllium target, was computed as $1/\sqrt{N}$, where N is the number of neutrons with a given energy in the spectrum; the calculation results are shown in Fig. 6. Clearly, the SEs of the neutron energy spectra are very small. The maximal SE values for the neutron peaks for ${}^{10}\text{B}$ in the different excited states are 2.49% and 2.31% for a deuteron energy of 250 keV and neutron emission angles of 0° and 45° , and 1.32% and 2.23% for a deuteron energy of 300 keV and neutron emission angles of 0° and 45° , respectively.

The energy resolution represents the ability of a TOF

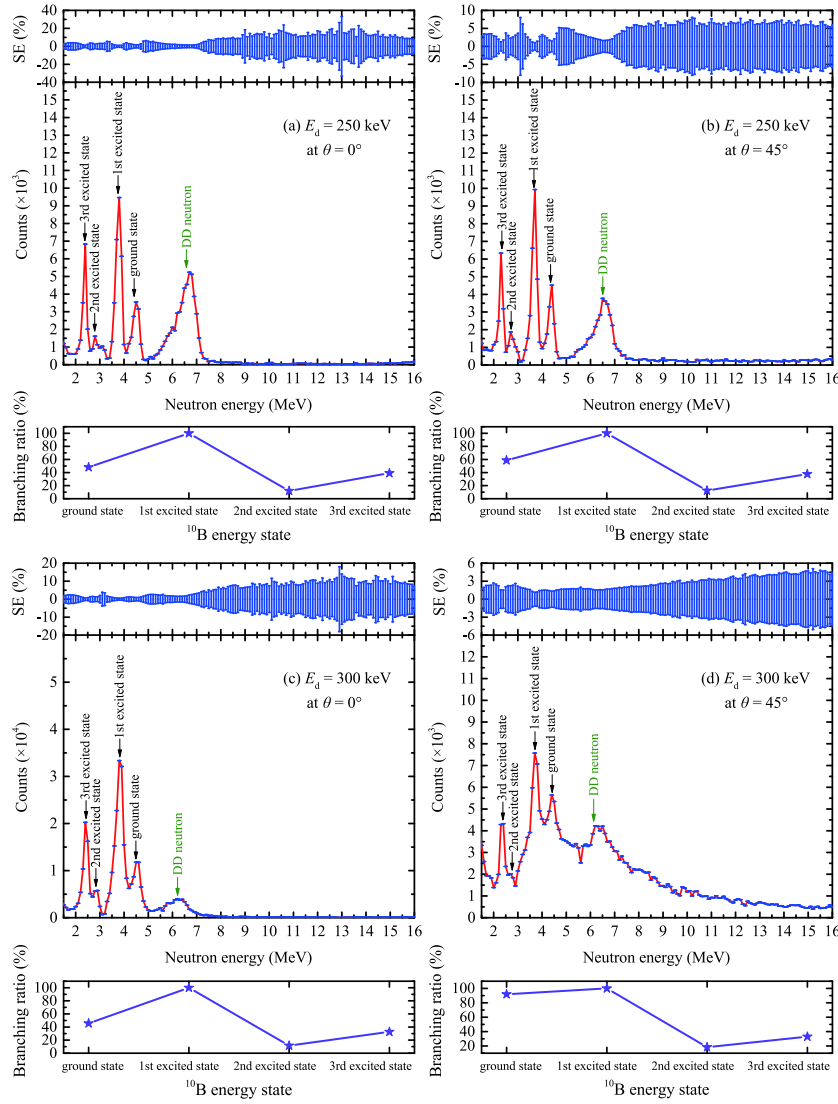


Fig. 6. (color online) The measured neutron energy spectra of the ${}^9\text{Be}(d,n){}^{10}\text{B}$ reaction, excluding the neutrons of the $\text{D}(d,n){}^3\text{He}$ reaction for the metallic beryllium target, for deuteron energies of 250 and 300 keV and neutron emission angles of 0° and 45° . The olive arrow denotes the neutrons from the $\text{D}(d,n){}^3\text{He}$ reaction, for the beam-limiting diaphragm. The black arrows indicate the neutrons from the ${}^9\text{Be}(d,n){}^{10}\text{B}$ reaction, for ${}^{10}\text{B}$ in different excited states.

spectrometer to discriminate neutrons with similar energies and can be defined as [41]

$$\frac{\Delta E}{E} = \frac{2\Delta t}{t} + \frac{2\Delta L}{L}, \quad (5)$$

where E is the neutron energy, ΔE is the full width at half maximum, t is the neutron TOF, and L is the neutron flight length ($L = 3.0$ m). ΔL is the uncertainty of the neutron flight distance, which is approximately 0.2 cm. Δt is given as

$$\Delta t = [(\Delta t_0)^2 + (\Delta t_h)^2 + (\Delta t_w)^2 + (\Delta t_s)^2 + (\Delta t_{\Delta E})^2]^{\frac{1}{2}}, \quad (6)$$

where Δt_0 is the time width of the pulse beam, which is

approximately 2.5 ns; Δt_h is the time uncertainty in the measurement owing to the crystal thickness of the scintillator detector, which can be calculated using $\Delta t_h = 1.837/\sqrt{E_n}$; Δt_w is the time uncertainty of the timing and time analyzer, which is approximately 0.5 ns; Δt_s is the uncertainty of the crossing time of the photomultiplier tube; and $\Delta t_{\Delta E}$ is the time uncertainty caused by the neutron energy divergence owing to the scattering of primary neutrons in the target chamber. Both Δt_s and $\Delta t_{\Delta E}$ can be neglected as they are small. Therefore, the uncertainty of the neutron TOF is $\Delta t = \sqrt{(6.5 \times E_n + 3.375)/E_n}$. The energy resolution as a function of the emitted neutron energy is shown in Fig. 7. Clearly, the neutron energy resolution of TOF is lower than 10% for neutron energies below 16 MeV.

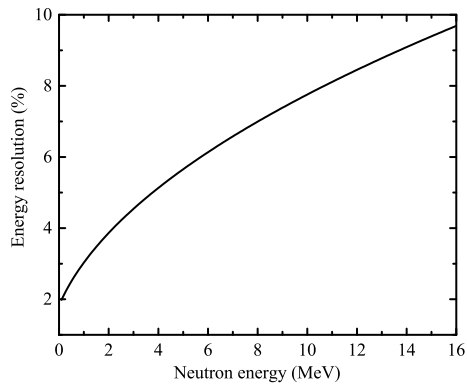


Fig. 7. The neutron energy resolution as a function of the energy of emitted neutrons considered in this work.

IV. CONCLUSION

The neutron energy spectra of the ${}^9\text{Be}(d,n){}^{10}\text{B}$ reaction with a thick beryllium target were measured using a fast neutron TOF spectrometer. The incident deuteron energies were 250 and 300 keV, and neutron emission angles were 0° and 45° . In this work, the neutrons from the $\text{D}(d,n){}^3\text{He}$ reaction for the metallic beryllium target were excluded from the neutron energy spectra of the

${}^9\text{Be}(d,n){}^{10}\text{B}$ reaction. However, the neutrons from the $\text{D}(d,n){}^3\text{He}$ reaction for the beam-limiting diaphragm were observed in the neutron energy spectra of the ${}^9\text{Be}(d,n){}^{10}\text{B}$ reaction, which did not affect the neutron energy spectra distribution of the ${}^9\text{Be}(d,n){}^{10}\text{B}$ reaction for different excited states of ${}^{10}\text{B}$.

The neutron contributions from the ${}^9\text{Be}(d,n){}^{10}\text{B}$ reaction were distributed relatively independently for different excited states of ${}^{10}\text{B}$, including the ground state, first excited state, second excited state, and third excited state of ${}^{10}\text{B}$. The branching ratios of the ${}^9\text{Be}(d,n){}^{10}\text{B}$ reaction for different excited states of ${}^{10}\text{B}$ were obtained for the neutron emission angles $\theta = 0^\circ$ and 45° , and the incident deuteron energies were 250 and 300 keV, respectively. With increasing incident deuteron energy, the branching ratio of the ${}^9\text{Be}(d,n){}^{10}\text{B}$ reaction for the third excited state clearly decreased. With increasing neutron emission angle, the branching ratios for the ground state and the second excited state increased. This work provides basic data for studying the physical mechanism of the ${}^9\text{Be}(d,n){}^{10}\text{B}$ reaction, and it provides the neutron energy distributions for low-energy-accelerator-based D-Be neutron sources used in neutron physics and neutron applications.

References

- [1] Z. E. Yao, W. M. Yue, P. Luo *et al.*, *Atomic Energy Science and Technology* **42**, 400 (2008)
- [2] Z. E. Yao, H. X. Du, X. J. Tan *et al.*, *Chinese Journal of Computational Physics* **25**, 744 (2008)
- [3] H. Koivunoro, D. L. Bleuel, U. Nastasi *et al.*, *Applied Radiation and Isotopes* **61**, 853 (2004)
- [4] Y. B. Nie, J. Ren, X. C. Ruan *et al.*, *Annals of Nuclear Energy* **136**, 107040 (2020)
- [5] Z. Wei *et al.*, *J Radioanal Nucl Chem* **305**, 455 (2015)
- [6] W. J. Li *et al.*, *Nucl. Sci. Tech.* **30**, 180 (2019)
- [7] X. J. Sun *et al.*, *Chin. Phys. Lett.* **36**, 112501 (2019)
- [8] J. J. Ma *et al.*, *Nucl. Sci. Tech.* **29**, 150 (2018)
- [9] M. Yiğit and E. Tel, *Nucl. Sci. Tech.* **28**, 165 (2017)
- [10] Z. Wei, Y. Yan *et al.*, *Phys. Rev. C* **87**, 054605 (2013)
- [11] Z. Wei, J. R. Wang *et al.*, *Chin. Phys. C* **43**, 054001 (2019)
- [12] J. F. Zhang, X. C. Ruan, L. Hou *et al.*, *High Power Laser and Particle Beams* **23**, 209 (2011)
- [13] R. Madey *et al.*, *Phys. Rev. C* **14**, 801 (1976)
- [14] J. W. Meadows, *Nucl. Instrum. Methods Phys. Res. A* **324**, 239 (1993)
- [15] Y. S. Park, A. Nüiler *et al.*, *Phys. Rev. C* **8**, 1557 (1973)
- [16] D. W. Glasgow *et al.*, *Nuclear Physics A* **99**, 170 (1967)
- [17] A. Belyam, A. Hoummada, J. Collot *et al.*, *Nucl. Instrum. Methods Phys. Res. B* **134**, 217 (1998)
- [18] F. M. Baumann, G. Domogala, H. Freiesleben *et al.*, *Nucl. Instrum. Methods Phys. Res. A* **247**, 359 (1986)
- [19] T. G. Miller *et al.*, *Phys. Rev. C* **1**, 763 (1970)
- [20] S. G. Buccino *et al.*, *Physics Letters* **19**, 234 (1965)
- [21] T. N. Massey, D. K. Jacobs, S. I. Al-Quraishi *et al.*, *Journal of Nuclear Science and Technology* **39**, 677 (2002)
- [22] D. L. Smith, J. W. Meadows, and P. T. Guenther, *Nucl. Instrum. Methods Phys. Res. A* **241**, 507 (1985)
- [23] S. Hashimoto, Y. Iwamoto, T. Sato *et al.*, *Progress in Nuclear Science and Technology* **4**, 418 (2014)
- [24] T. N. Massey, T. W. Covell, S. I. Al-Quraishi *et al.*, *Fusion Engineering and Design* **37**, 57 (1997)
- [25] S. Whittlestone, *Journal of Physics D: Applied Physics* **10**, 1715 (1977)
- [26] Y. Iwamoto, Y. Sakamoto, N. Matsuda *et al.*, *Nucl. Instrum. Methods Phys. Res. A* **598**, 687 (2009)
- [27] H. J. Brede, G. Dietze, K. Kudo *et al.*, *Nucl. Instrum. Methods Phys. Res. A* **274**, 332 (1989)
- [28] T. Inada, K. Kawachi, and T. Hiramoto, *Journal of Nuclear Science and Technology* **5**, 22 (1968)
- [29] X. Z. Wang *et al.*, *Nuclear Science and Techniques* **5**, 193 (1994)
- [30] K. A. Weaver *et al.*, *Phys. Med. Biol.* **18**, 64 (1973)
- [31] K. A. Weaver, J. D. Anderson, H. H. Barschall *et al.*, *Nuclear Science and Engineering* **52**, 35 (1973)
- [32] M. A. Lone, C. B. Bigham, J. S. Fraser *et al.*, *Nuclear Instruments and Methods* **143**, 331 (1977)
- [33] S. Nakayama *et al.*, *Phys. Rev. C* **94**, 014618 (2016)
- [34] J. G. XU, H. Li *et al.*, *Nuclear Techniques* **31**, 814 (2008)
- [35] M. E. Capoulat, N. Sauzet, A. A. Valda *et al.*, *Nucl. Instrum. Methods Phys. Res. B* **445**, 57 (2019)
- [36] M. Stefanik, P. Bem, M. Majerle *et al.*, *Radiation Physics and Chemistry* **140**, 466 (2017)
- [37] R. A. Coombe *et al.*, *Proc. Phys. Soc.* **80**, 1218 (1962)
- [38] Y. B. Zou, Y. Y. Pei, D. W. Mo *et al.*, FNDA, 058(2006)
- [39] G. Dietze and H. Klein, Report PTB-ND-22, (1982)
- [40] D. Chen and W. B. Jia, *Applied Neutron Physics*, First edition (Beijing: Science Press, 2015), p.21 (in Chinese)
- [41] G. R. Shen, *Neutron Flight Time Method and Application*, First edition (Beijing: Atomic Energy Press, 2007), p.108 (in Chinese)